

Bilayer two-orbital model of $\text{La}_3\text{Ni}_2\text{O}_7$ under pressure

Zhihui Luo,^{1,*} Xunwu Hu,^{1,*} Meng Wang,¹ Wéi Wú,¹ and Dao-Xin Yao^{1,†}

¹Center for Neutron Science and Technology, Guangdong Provincial Key Laboratory of Magnetoelectric Physics and Devices, State Key Laboratory of Optoelectronic Materials and Technologies, School of Physics, Sun Yat-Sen University, Guangzhou, 510275, China
(Dated: May 26, 2023)

The newly discovered Ruddlesden-Popper bilayer $\text{La}_3\text{Ni}_2\text{O}_7$ reaches an remarkable superconducting transition temperature $T_c = 80$ K under a pressure of above 14 GPa. Here we propose a minimal bilayer two-orbital model of the high-pressure phase of $\text{La}_3\text{Ni}_2\text{O}_7$. Our model is constructed with the $\text{Ni}-3d_{x^2-y^2}$, $3d_{3z^2-r^2}$ orbitals by using Wannier downfolding of the DFT calculations, which captures the key ingredients of the material, such as band structure and Fermi surface topology. There are one hole pocket γ and two electron pockets α, β on the Fermi surface, in which the α, β pockets show mixing of two orbitals, while the γ -pocket is associated with $\text{Ni}-d_{3z^2-r^2}$ orbital. The RPA spin susceptibility reveals a magnetic enhancement associating to the $d_{3z^2-r^2}$ state. A higher energy model with $\text{O}-p$ orbitals is also provided for further study.

Introduction.—Recently the newly discovered Ruddlesden-Popper bilayer perovskite nickelate $\text{La}_3\text{Ni}_2\text{O}_7$ shows a remarkable high superconducting transition temperature of $T_c = 80$ K with an applied pressure of over 14 GPa [1]. This breakthrough will undoubtedly provoke a stir in the field of high- T_c superconductivity (hsTC) long after the discovery of cuprate [2–7] and iron-based [8–11], as well as the recent infinite layer Nickelate superconductors [12–34]. At ambient pressure, $\text{La}_3\text{Ni}_2\text{O}_7$ exhibits an orthorhombic structure of Amam space group [35]. With increasing pressure, it undergoes a structure transition to Fmmm space group, which possesses a more regular AA-stacking structure with apical Ni-O-Ni bond approaching 180° [see Figs. 1f, g in Ref. [1]]. The most crucial effect of the pressure is to drive a metallic transition of the correlated electronic ground state [36–39]. The resistance measurement shows that, above T_c , $\text{La}_3\text{Ni}_2\text{O}_7$ undergoes a transition from weakly insulating to metallic phase [see Figs. 3a, 4 in Ref. [1]], which is further evidenced in the density functional theory (DFT) calculation as the emergence of an additional $\text{Ni}-d_{3z^2-r^2}$ state near Fermi energy (E_F). Such a state is essentially associated to the σ -bonding that connects $\text{Ni}-d_{3z^2-r^2}$ and apical $\text{O}-p_z$ orbitals, further indicating a rather different situation in $\text{La}_3\text{Ni}_2\text{O}_7$ in which the unconventional pairing might be promoted by such a coupling degree [40, 41]. Therefore, it is of vital at once to understand the effective low-energy physics.

In this paper, we propose a bilayer two-orbital model for the high-pressure phase of $\text{La}_3\text{Ni}_2\text{O}_7$. Our models is constructed based on Wannier downfolding of the DFT band structure, which capture key feature of electronic structure at E_F and could serve as a starting for further strongly correlated calculations and investigation on the unconventional pairing symmetry.

Electronic model.— To simplify elucidate the electronic structure of $\text{La}_3\text{Ni}_2\text{O}_7$ under the high-pressure phase (29.5 Gpa), a primitive unit cell with two-Ni atoms is

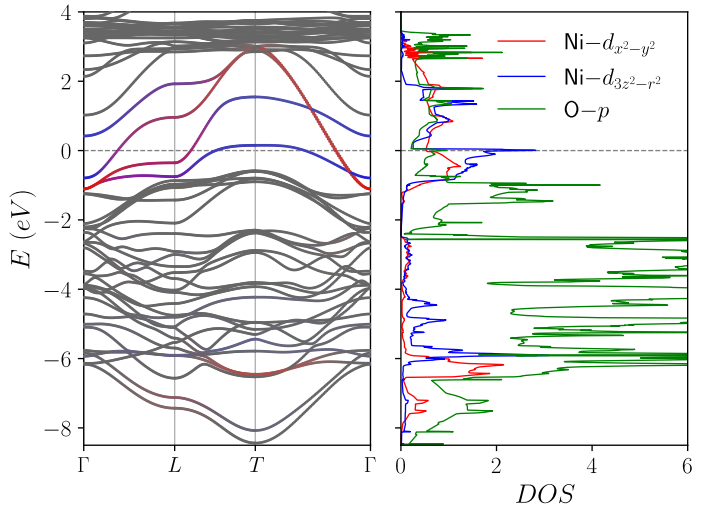


FIG. 1. The DFT band structure and partial density of states of the high-pressure Fmmm phase of $\text{La}_3\text{Ni}_2\text{O}_7$. The blue, red and green colors represent $\text{Ni}-d_{x^2-y^2}$, $d_{3z^2-r^2}$ and $\text{O}-p$ states, respectively.

adopted. We fix the experimentally refined lattice parameters [1] and fully optimize the atomic positions using the DFT as implemented in the Vienna *ab initio* simulation package (VASP) [42, 43]. The projector augmented-wave (PAW) method [44] with a 600 eV plane-wave cut-off is adopted. The generalized gradient approximation (GGA) of Perdew-Burke-Ernzerhof (PBE) [45] is used for exchange-correlation functional. In Fig. ?? we show the resulting band structure and partial density of states, which distinctly shows a major $\text{Ni}-d_{x^2-y^2}$ and $d_{3z^2-r^2}$ near E_F . Note that there appears a hole pocket associating $\text{Ni}-d_{3z^2-r^2}$ orbital at T point. This hole pocket is separated from the other one upper the Fermi surface with an energy ~ 1.3 eV. This splitting should be attributed to $pd\sigma$ -bonding between $\text{Ni}-d_{3z^2-r^2}$ and apical $\text{O}-p_z$ orbitals.

t_1^x	t_1^z	t_2^x	t_2^z	t_3^{xz}
-0.483	-0.110	0.069	-0.017	0.239
t_\perp^x	t_\perp^z	t_4^{xz}	ϵ^x	ϵ^z
0.005	-0.635	-0.034	0.495	0.882

TABLE I. Tight-binding parameters of the bilayer two-orbital model. The hoppings t are demonstrated in Fig. 2a. ϵ^x, ϵ^z are site energies for $\text{Ni}-d_{x^2-y^2}, d_{3z^2-r^2}$ orbitals, respectively.

With the Wannier downfolding [46–48], we arrive at an effective bilayer two-orbital model

$$\begin{aligned}\mathcal{H} &= \mathcal{H}_0 + \mathcal{H}_U, \\ \mathcal{H}_0 &= \sum_{\mathbf{k}\sigma} \Psi_{\mathbf{k}\sigma}^\dagger H(\mathbf{k}) \Psi_{\mathbf{k}\sigma}, \\ \mathcal{H}_U &= U \sum_{is} n_{is\uparrow} n_{is\downarrow} \\ &\quad + \sum_{i\alpha\beta} (U' - J\delta_{\alpha\beta}) (n_{iA\alpha} n_{iA\beta} + n_{iB\alpha} n_{iB\beta}).\end{aligned}\quad (1)$$

Here \mathcal{H}_0 is the tight-binding Hamiltonian determined out of our Wannier downfolding, and \mathcal{H}_U is the Coulomb interaction term [49]. The basis is defined as $\Psi_\sigma = (d_{Ax\sigma}, d_{Az\sigma}, d_{Bx\sigma}, d_{Bz\sigma})^T$, with the field operator $d_{s\sigma}$ denotes annihilation of an $s = Ax, Az, Bx, Bz$ electron with spin σ . As shown in Fig. 2, A, B label the bilayer, and x, z label $d_{x^2-y^2}, d_{3z^2-r^2}$ orbitals, respectively. For \mathcal{H}_U , U, U', J are intra-orbital, inter-orbital Coulomb repulsion and Hund coupling, respectively. The matrix $H(\mathbf{k})$ is written as

$$\begin{aligned}H(\mathbf{k}) &= \begin{pmatrix} H_A(\mathbf{k}) & H_{AB}(\mathbf{k}) \\ H_{AB}(\mathbf{k}) & H_A(\mathbf{k}) \end{pmatrix}, \\ H_A(\mathbf{k}) &= \begin{pmatrix} T_k^x & V_k \\ V_k & T_k^z \end{pmatrix}, \quad H_{AB}(\mathbf{k}) = \begin{pmatrix} t_\perp^x & V_k' \\ V_k' & t_\perp^z \end{pmatrix}.\end{aligned}\quad (2)$$

with

$$\begin{aligned}T_k^{x/z} &= 2t_1^{x/z} (\cos k_x + \cos k_y) + 4t_2^{x/z} \cos k_x \cos k_y + \epsilon^{x/z}, \\ V_k &= 2t_3^{xz} (\cos k_x - \cos k_y), \quad V_k' = 2t_4^{xz} (\cos k_x - \cos k_y).\end{aligned}$$

Here $T_k^{x/z}$ represents intra-layer intra-orbital hopping, and V_k (V_k') represent intra-layer (inter-layer) hybridization between $d_{x^2-y^2}$ and $d_{3z^2-r^2}$ orbitals. The essential hoppings $t_1^{x/z}, t_2^{x/z}, t_3^{xz}, t_4^{xz}$ are demonstrated in Fig. 2a. Note that the minus sign appeared in t_3^{xz}, t_4^{xz} is associated to the orbital symmetry of two e_g orbitals. Meanwhile, these parameters are not fully independent according to Slater-Koster integrals [50]. For example, for nearest-neighbor hoppings, there are relation $t_1^x = (3V_\sigma + V_\delta)/4$, $t_1^z = (V_\sigma + 3V_\delta)/4$, $t_3^{xz} = \sqrt{3}(V_\delta - V_\sigma)/4$, with V_σ, V_δ the corresponding dd bonding.

To better illustrate the low-energy state, it is advisable to further simplify the above model. Recall that

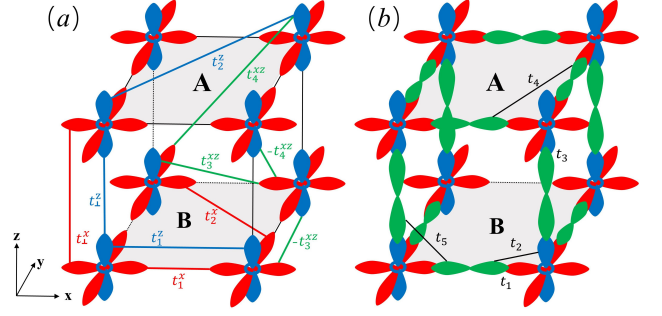


FIG. 2. Schematic of the bilayer $\text{La}_3\text{Ni}_2\text{O}_7$ lattice with hopping parameters. (a) Only $\text{Ni}-d_{x^2-y^2}$ (red), $d_{3z^2-r^2}$ (blue) orbitals are shown. The blue, red, green lines indicate hoppings of the bilayer two-orbital model. Their values are listed in Tabel I. (b) Extra O- p orbitals are drawn as green shapes, with in-plane p_x, p_y and apical p_z . The hopping parameters are given in Tabel II.

the mirror symmetry of the bilayer structure allows us to define the bonding and anti-bonding states $\Phi_{\pm\mathbf{k}\sigma} = (c_{\pm\mathbf{k}\sigma}^x, c_{\pm\mathbf{k}\sigma}^z)^T$ with $c_{\pm\mathbf{k}\sigma}^{x/z} = \frac{1}{\sqrt{2}} (d_{\mathbf{k}A\sigma}^{x/z} \pm d_{\mathbf{k}B\sigma}^{x/z})$, in which the Hamiltonian acquires a block-diagonal form

$$\begin{aligned}\mathcal{H}_0 &= \sum_{\mathbf{k}\sigma} \left(\Phi_{+\mathbf{k}\sigma}^\dagger H_+(\mathbf{k}) \Phi_{+\mathbf{k}\sigma} + \Phi_{-\mathbf{k}\sigma}^\dagger H_-(\mathbf{k}) \Phi_{-\mathbf{k}\sigma} \right), \\ H_\pm(\mathbf{k}) &= \begin{pmatrix} T_k^x \pm t_\perp^x & V_k \pm V_k' \\ V_k \pm V_k' & T_k^z \pm t_\perp^z \end{pmatrix}.\end{aligned}\quad (3)$$

In this representation, the two $d_{3z^2-r^2}$ states at E_F are manifested as the component $T_k^z \pm t_\perp^z$ which define a splitting energy $2t_\perp^z$.

With the value of hopping parameters listed in Tabel I, we show in Fig. 3 the resulting band structure and Fermi surface. The model reproduces the DFT band structure well at E_F . In Fig. 3b we can see one hole pocket γ and two electron pockets α, β . The α, β -pocket show mixing of orbital content, while the γ -pocket is featured as a dominated $d_{3z^2-r^2}$ state. Note that the amplitude of $t_\perp^z = -0.635$ is even larger than that of the intra-layer nearest-neighbor hopping $t_1^x = -0.483$, by a ratio of 1.31. This strong inter-layer coupling could pass their effect to the $d_{x^2-y^2}$ orbital through hybridization V_k, V_k' , leading to a possible different situation of the unconventional pairing as compared to cuprates. This is in reminiscent of the bilayer-Hubbard model [51], in which an s_\pm -wave pairing could be promoted via inter-layer coupling. We would also like to point out that, however, due to the asymmetry of orthorhombic structure of this compound, the γ -pocket from DFT is slightly stretched along nodal direction.

To explicitly include the physics of O- p orbitals, we introduce a higher energy model (nine-orbital model) based on the bilayer two-orbital model. The basis is $\Psi_\sigma = (d_{Ax\sigma}, d_{Az\sigma}, d_{Bx\sigma}, d_{Bz\sigma}, p_{Ax\sigma}, p_{Ay\sigma}, p_{Bx\sigma}, p_{By\sigma}, p_{z\sigma})^T$, with four new in-plane p_x, p_y and one apical p_z included.

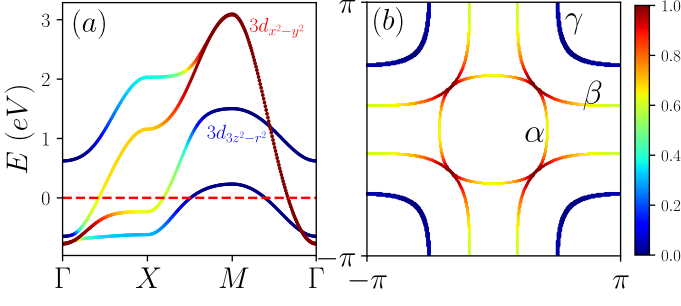


FIG. 3. The band structure (a) and Fermi surface (b) of the bilayer two-orbital model. The colorbar indicates the orbital weight of $d_{x^2-y^2}$ and $d_{3z^2-r^2}$.

t_1	t_2	t_3	t_4	t_5	ϵ^x	ϵ^z
1.564	-0.747	-1.625	-0.577	0.487	-1.057	-1.161
ϵ_p^x	ϵ_p^y	ϵ_p^z				
-4.936	-4.936	-4.294				

TABLE II. Tight-binding parameters for Wannier downfolding of the nine-orbital model. ϵ are the site energies for Ni- $d_{x^2-y^2}$, $d_{3z^2-r^2}$ and O- p orbitals, as indicated in Fig. 2b.

The tight-binding parameters of the model are listed in Tabel II, which requires only five hopping parameters shown in Fig. 2b. The nine-orbital model can also reproduced the major features of the band structure and Fermi surface at E_F , which will be useful for further study of the electronic correlation in the dynamic mean field theory calculation.

Spin susceptibility.—To determine the magnetic response of the material, we investigate the the spin susceptibility of our model, which is defined as

$$\chi_S^{st}(q, i\omega_n) = \frac{1}{3} \int_0^\beta d\tau e^{i\omega_n \tau} \langle S_s(q, \tau) \cdot S_t(-q, 0) \rangle. \quad (4)$$

Here $s, t = Ax, Az, Bx, Bz$ label orbitals, and the spin operator is defined as $S_{qs} = \frac{1}{2} \sum_{k\alpha\beta} d_{ks\alpha}^\dagger \boldsymbol{\sigma}_{\alpha\beta} d_{k+qs\beta}$ with $\boldsymbol{\sigma}$ the Pauli matrix. By using wick theorem, we expand Eq. 4 to obtain the bare (non-interacting) susceptibility

$$\chi_S^{st}(q, i\omega_n) = -\frac{1}{2N} \sum_{mn} \frac{f(\epsilon_k^n) - f(\epsilon_k^m)}{i\omega_n + \epsilon_k^n - \epsilon_{k+q}^m} \times \langle m|k+qt\rangle \langle k+qs|m\rangle \langle n|ks\rangle \langle kt|n\rangle,$$

with m, n the band indices and $f(\epsilon) = \frac{1}{e^{\epsilon/T} + 1}$ the Fermi-Dirac function. $\langle ks|m\rangle$ represents the eigenvector relating s, m states at wave vector k .

Under the random phase approximation, the spin susceptibility is calculated by

$$\chi_S^{st, \text{RPA}}(q, i\omega_n) = [I - \chi_S^{st}(q, i\omega_n)\Gamma]^{-1} \chi_S^{st}(q, i\omega_n), \quad (5)$$

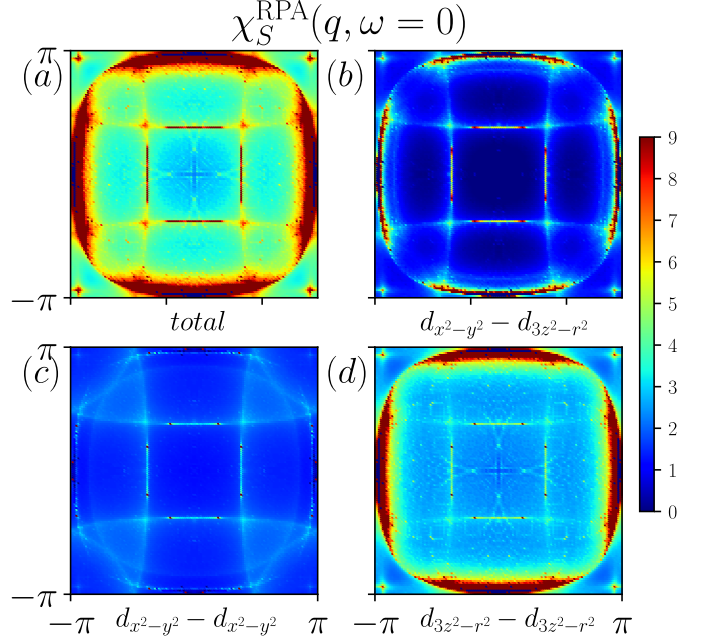


FIG. 4. Spin susceptibility $\chi_S^{st, \text{RPA}}(q, \omega = 0)$ of the bilayer two-orbital model. (a) The total orbital sum $\chi_S^{\text{RPA}} = \sum_{st} \chi_S^{st, \text{RPA}}$ which corresponds to the experimental measurable. (b-d) Orbital-resolved $\chi_S^{st, \text{RPA}}$. An amplified factor of 2 is used in (b-c).

with interaction vertex defined as

$$\Gamma = \begin{pmatrix} 1 & \\ & 1 \end{pmatrix} \otimes \begin{pmatrix} U & J/2 \\ J/2 & U \end{pmatrix}.$$

In Fig. 4 we show the constant energy slices of $\chi_S^{\text{RPA}}(q, \omega = 0)$. Here we use $U = 3, J = 0.4$ eV. $T = 0$ is applied since temperature only trivially brings a broadening to the spectrum. Fig. 4a is the total $\chi_S^{\text{RPA}} = \sum_{s,t} \chi_S^{st, \text{RPA}}$ corresponding to experimental measurable. As can be seen, the magnetic signal shows a ring-like enhancement and intersects at $X = (\pi, 0)$ point, which might suggests a stripe spin density wave instability. To unveil the origin, we show in Figs. 4b-d the orbital-resolved $\chi_S^{st, \text{RPA}}$, from which we can see a dominated intra-orbital $d_{3z^2-r^2}$ scattering reflecting the Fermi surface nesting of γ -pocket. While the signal from other two channels are weaker, consisting with the strong orbital mixing in α, β -pockets. Our result could be further tested in the magnetic measurement.

Discussion.— The discovery of the high transition temperature superconductor $\text{La}_3\text{Ni}_2\text{O}_7$ represents a major breakthrough in the field of nickelate superconductivity. Our DFT calculations demonstrate that there are one hole pocket γ and two electron pockets α, β on the Fermi surface, in which the α, β -pockets exhibit mixing of orbitals, while the γ -pocket features a dominated $d_{3z^2-r^2}$ component. In comparison to the bulk Ni-112,

which has not yet demonstrated a finite T_c , $\text{La}_3\text{Ni}_2\text{O}_7$ exhibits several distinguishing features that may be crucial to superconductivity. First, the less correlated La-5d derived bands are expelled from the Fermi level, diminishing the hybridization between the Ni-3d_{x²-y²} and La-5d orbitals that impedes superconductivity. Furthermore, the site energy difference between Ni-d_{x²-y²} and O-p in $\text{La}_3\text{Ni}_2\text{O}_7$ is estimated as $\Delta \equiv \epsilon_d - \epsilon_p = 3.88$ eV. This value is smaller than that of RNiO_2 (4.4 eV), which could potentially contribute to the high T_c in $\text{La}_3\text{Ni}_2\text{O}_7$ in the context of pairing based on Zhang-Rice singlet state [52]. The inclusion of the $d_{3z^2-r^2}$ near Fermi level in $\text{La}_3\text{Ni}_2\text{O}_7$, however, may have complex implications for superconductivity. The large density of state of $d_{3z^2-r^2}$ orbital can provide new phase space for the potential pairing of electrons. However, the presence of multiple orbitals on Fermi level may also lead to competition between pairings with different symmetries, such as the competition between $d_{x^2-y^2}$ and s_{\pm} wave pairing. Regarding the filling factors of the relevant orbitals, we note that in the case of a $d^{7.5}$ configuration of Ni, if $d_{3z^2-r^2}$ is considered to roughly have the same occupation number of $d_{x^2-y^2}$, then both orbitals have about 0.75 electrons per site, corresponding to 25% hole-doping in the NiO_2 plane. It is notable that the oxygen-deficient in realistic materials may effectively reduce the hole doping level in e_g orbitals of Ni-3d, resulting enhanced superconductivity. Finally, we acknowledge that the $d_{3z^2-r^2}$ orbitals exhibit much weaker hybridization with in-plane oxygen compared to its $d_{x^2-y^2}$ counterpart, which necessitates in-depth investigations into its strong interaction effects and its influence on superconductivity. The question about the role of the electron-phonon coupling, which becomes specifically important since the superconductivity in $\text{La}_3\text{Ni}_2\text{O}_7$ is found under pressure, should also be clarified in future studies.

Conclusion.— In conclusion, we have introduced a minimal bilayer two-orbital model for the Ruddlesden-Popper bilayer $\text{La}_3\text{Ni}_2\text{O}_7$ under pressure. The tight-binding parameters are obtained by Wannier downfolding of the DFT calculations, which reproduce the band structure and Fermi surface well. The spin susceptibility is studied using the RPA method based on the model, which shows the magnetic signal is majorly comes from $d_{3z^2-r^2}$. This model provides important means to the study of electronic, magnetic, orbital, and superconducting properties of the material under pressure.

We thank the useful discussions with Guang-Ming Zhang and Biao Lv. Work at Sun Yat-Sen University was supported by the National Key Research and Development Program of China (Grants No. 2022YFA1402802, 2018YFA0306001), the National Natural Science Foundation of China (Grants No. 92165204, No.12174454, No. 11974432, No.12274472), the Guangdong Basic and Applied Basic Research Foundation (Grants No. 2022A1515011618, No. 2021B1515120015), Guang-

dong Provincial Key Laboratory of Magnetoelectric Physics and Devices (Grant No. 2022B1212010008), Shenzhen International Quantum Academy (Grant No. SIQA202102), and Leading Talent Program of Guangdong Special Projects (201626003).

* These authors contributed equally to this work

† yaodaax@mail.sysu.edu.cn

- [1] H. Sun, M. Huo, X. Hu, J. Li, Y. Han, L. Tang, Z. Mao, P. Yang, B. Wang, J. Cheng, *et al.*, Superconductivity near 80 kelvin in single crystals of $\text{La}_3\text{Ni}_2\text{O}_7$ under pressure, [arXiv:2305.09586 \(2023\)](#).
- [2] J. G. Bednorz and K. A. Müller, Possible high T_c superconductivity in the Ba-La-Cu-O system, *Zeitschrift für Physik B Condensed Matter* **64**, 189 (1986).
- [3] P. W. Anderson, The resonating valence bond state in La_2CuO_4 and superconductivity, *Science* **235**, 1196 (1987).
- [4] P. A. Lee, N. Nagaosa, and X.-G. Wen, Doping a mott insulator: Physics of high-temperature superconductivity, *Rev. Mod. Phys.* **78**, 17 (2006).
- [5] B. Keimer, S. A. Kivelson, M. R. Norman, S. Uchida, and J. Zaanen, From quantum matter to high-temperature superconductivity in copper oxides, *Nature* **518**, 179 (2015).
- [6] H. Sakakibara, K. Suzuki, H. Usui, S. Miyao, I. Maruyama, K. Kusakabe, R. Arita, H. Aoki, and K. Kuroki, Orbital mixture effect on the fermi-surface- T_c correlation in the cuprate superconductors: Bilayer vs. single layer, *Phys. Rev. B* **89**, 224505 (2014).
- [7] W. Li, J. Zhao, L. Cao, Z. Hu, Q. Huang, X. Wang, Y. Liu, G. Zhao, J. Zhang, Q. Liu, *et al.*, Superconductivity in a unique type of copper oxide, *Proceedings of the National Academy of Sciences* **116**, 12156 (2019).
- [8] S. Raghu, X.-L. Qi, C.-X. Liu, D. J. Scalapino, and S.-C. Zhang, Minimal two-band model of the superconducting iron oxypnictides, *Phys. Rev. B* **77**, 220503 (2008).
- [9] A. V. Chubukov, D. V. Efremov, and I. Eremin, Magnetism, superconductivity, and pairing symmetry in iron-based superconductors, *Phys. Rev. B* **78**, 134512 (2008).
- [10] H. Eschrig and K. Koepernik, Tight-binding models for the iron-based superconductors, *Phys. Rev. B* **80**, 104503 (2009).
- [11] M. Daghofer, A. Nicholson, A. Moreo, and E. Dagotto, Three orbital model for the iron-based superconductors, *Phys. Rev. B* **81**, 014511 (2010).
- [12] D. Li, K. Lee, B. Y. Wang, M. Osada, S. Crossley, H. R. Lee, Y. Cui, Y. Hikita, and H. Y. Hwang, Superconductivity in an infinite-layer nickelate, *Nature* **572**, 624 (2019).
- [13] E. Been, W.-S. Lee, H. Y. Hwang, Y. Cui, J. Zaanen, T. Devereaux, B. Moritz, and C. Jia, Electronic structure trends across the rare-earth series in superconducting infinite-layer nickelates, *Phys. Rev. X* **11**, 011050 (2021).
- [14] J. Zaanen and P. B. Littlewood, Freezing electronic correlations by polaronic instabilities in doped La_2NiO_4 , *Phys. Rev. B* **50**, 7222 (1994).
- [15] J. M. Tranquada, D. J. Buttrey, V. Sachan, and J. E. Lorenzo, Simultaneous ordering of holes and spins in $\text{La}_2\text{NiO}_{4.125}$, *Phys. Rev. Lett.* **73**, 1003 (1994).

- [16] K.-W. Lee and W. E. Pickett, Infinite-layer LaNiO_2 : ni^{1+} is not cu^{2+} , *Phys. Rev. B* **70**, 165109 (2004).
- [17] M. Hepting, D. Li, C. Jia, H. Lu, E. Paris, Y. Tseng, X. Feng, M. Osada, E. Been, Y. Hikita, *et al.*, Electronic structure of the parent compound of superconducting infinite-layer nickelates, *Nature materials* **19**, 381 (2020).
- [18] A. S. Botana and M. R. Norman, Similarities and differences between lanio_2 and cacuo_2 and implications for superconductivity, *Phys. Rev. X* **10**, 011024 (2020).
- [19] X. Wu, D. Di Sante, T. Schwemmer, W. Hanke, H. Y. Hwang, S. Raghu, and R. Thomale, Robust $d_{x^2-y^2}$ -wave superconductivity of infinite-layer nickelates, *Phys. Rev. B* **101**, 060504 (2020).
- [20] M. Jiang, M. Berciu, and G. A. Sawatzky, Critical nature of the ni spin state in doped ndnio_2 , *Phys. Rev. Lett.* **124**, 207004 (2020).
- [21] L.-H. Hu and C. Wu, Two-band model for magnetism and superconductivity in nickelates, *Phys. Rev. Res.* **1**, 032046 (2019).
- [22] Y. Nomura, M. Hirayama, T. Tadano, Y. Yoshimoto, K. Nakamura, and R. Arita, Formation of a two-dimensional single-component correlated electron system and band engineering in the nickelate superconductor ndnio_2 , *Phys. Rev. B* **100**, 205138 (2019).
- [23] G.-M. Zhang, Y.-f. Yang, and F.-C. Zhang, Self-doped mott insulator for parent compounds of nickelate superconductors, *Phys. Rev. B* **101**, 020501 (2020).
- [24] Y.-H. Zhang and A. Vishwanath, Type-ii t - j model in superconducting nickelate $\text{nd}_{1-x}\text{sr}_x\text{nio}_2$, *Phys. Rev. Res.* **2**, 023112 (2020).
- [25] P. Werner and S. Hoshino, Nickelate superconductors: Multiorbital nature and spin freezing, *Phys. Rev. B* **101**, 041104 (2020).
- [26] F. Bernardini, V. Olevano, and A. Cano, Magnetic penetration depth and T_c in superconducting nickelates, *Phys. Rev. Res.* **2**, 013219 (2020).
- [27] Y. Gu, S. Zhu, X. Wang, J. Hu, and H. Chen, A substantial hybridization between correlated ni-d orbital and itinerant electrons in infinite-layer nickelates, *Communications Physics* **3**, 84 (2020).
- [28] M. Kitatani, L. Si, O. Janson, R. Arita, Z. Zhong, and K. Held, Nickelate superconductors—a renaissance of the one-band hubbard model, *npj Quantum Materials* **5**, 59 (2020).
- [29] F. Lechermann, Doping-dependent character and possible magnetic ordering of ndnio_2 , *Phys. Rev. Mater.* **5**, 044803 (2021).
- [30] A. Kreisel, B. M. Andersen, A. T. Rømer, I. M. Eremin, and F. Lechermann, Superconducting instabilities in strongly correlated infinite-layer nickelates, *Phys. Rev. Lett.* **129**, 077002 (2022).
- [31] F. Lechermann, Multiorbital processes rule the $\text{nd}_{1-x}\text{sr}_x\text{nio}_2$ normal state, *Phys. Rev. X* **10**, 041002 (2020).
- [32] V. Pardo and W. E. Pickett, Metal-insulator transition in layered nickelates $\text{la}_3\text{ni}_2\text{o}_{7-\delta}$ ($\delta = 0.0, 0.5, 1$), *Phys. Rev. B* **83**, 245128 (2011).
- [33] M. Nakata, D. Ogura, H. Usui, and K. Kuroki, Finite-energy spin fluctuations as a pairing glue in systems with coexisting electron and hole bands, *Phys. Rev. B* **95**, 214509 (2017).
- [34] N. Kitamine, M. Ochi, and K. Kuroki, Designing nickelate superconductors with d^8 configuration exploiting mixed-anion strategy, *Phys. Rev. Res.* **2**, 042032 (2020).
- [35] Z. Liu, H. Sun, M. Huo, X. Ma, Y. Ji, E. Yi, L. Li, H. Liu, J. Yu, Z. Zhang, *et al.*, Evidence for charge and spin density waves in single crystals of $\text{La}_3\text{Ni}_2\text{O}_7$ and $\text{La}_3\text{Ni}_2\text{O}_6$, *Science China Physics, Mechanics & Astronomy* **66**, 217411 (2023).
- [36] H. J. Choi, D. Roundy, H. Sun, M. L. Cohen, and S. G. Louie, The origin of the anomalous superconducting properties of MgB_2 , *Nature* **418**, 758 (2002).
- [37] M. Gao, Z.-Y. Lu, and T. Xiang, Prediction of phonon-mediated high-temperature superconductivity in $\text{li}_3\text{b}_4\text{c}_2$, *Phys. Rev. B* **91**, 045132 (2015).
- [38] A. Drozdov, P. Kong, V. Minkov, S. Besedin, M. Kuzovnikov, S. Mozaffari, L. Balicas, F. Balakirev, D. Graf, V. Prakapenka, *et al.*, Superconductivity at 250 k in lanthanum hydride under high pressures, *Nature* **569**, 528 (2019).
- [39] M. Gao, Z. Lu, and T. Xiang, Finding high-temperature superconductors by metallizing the σ -bonding electrons, *PHYSICS* **44**, 421 (2015).
- [40] J. Hu, Identifying the genes of unconventional high temperature superconductors, *Science bulletin* **61**, 561 (2016).
- [41] J. Hu, C. Le, and X. Wu, Predicting unconventional high-temperature superconductors in trigonal bipyramidal coordinations, *Phys. Rev. X* **5**, 041012 (2015).
- [42] G. Kresse and J. Hafner, Ab initio molecular dynamics for liquid metals, *Phys. Rev. B* **47**, 558 (1993).
- [43] G. Kresse and J. Furthmüller, Efficient iterative schemes for ab initio total-energy calculations using a plane-wave basis set, *Phys. Rev. B* **54**, 11169 (1996).
- [44] P. E. Böchl, Projector augmented-wave method, *Phys. Rev. B* **50**, 17953 (1994).
- [45] J. P. Perdew, K. Burke, and M. Ernzerhof, Generalized gradient approximation made simple, *Phys. Rev. Lett.* **77**, 3865 (1996).
- [46] G. P. et al., Wannier90 as a community code: new features and applications, *Journal of Physics: Condensed Matter* **32**, 165902 (2020).
- [47] N. Marzari and D. Vanderbilt, Maximally localized generalized wannier functions for composite energy bands, *Phys. Rev. B* **56**, 12847 (1997).
- [48] I. Souza, N. Marzari, and D. Vanderbilt, Maximally localized wannier functions for entangled energy bands, *Phys. Rev. B* **65**, 035109 (2001).
- [49] A. Georges, L. d. Medici, and J. Mravlje, Strong correlations from hunds coupling, *Annual Review of Condensed Matter Physics* **4**, 137 (2013).
- [50] J. C. Slater and G. F. Koster, Simplified LCAO method for the periodic potential problem, *Phys. Rev.* **94**, 1498 (1954).
- [51] T. A. Maier and D. J. Scalapino, Pair structure and the pairing interaction in a bilayer hubbard model for unconventional superconductivity, *Phys. Rev. B* **84**, 180513 (2011).
- [52] F. C. Zhang and T. M. Rice, Effective hamiltonian for the superconducting cu oxides, *Phys. Rev. B* **37**, 3759 (1988).